Measurement of the $^{12}C(e,e'p)^{11}B$ two-body breakup reaction at high missing momentum

2014 J. Phys. G: Nucl. Part. Phys. 41 105109

(http://iopscience.iop.org/0954-3899/41/10/105109)

IOP Publishing Journal of Physics G: Nuclear and Particle Physics

J. Phys. G: Nucl. Part. Phys. **41** (2014) 105109 (11pp) doi:10.1088/0954-3899/41/10/105109

Measurement of the $^{12}C(e,e'p)^{11}B$ two-body breakup reaction at high missing momentum

P Monaghan[1,2], R Shneor[3], R Subedi[4], B D Anderson[4], K Aniol[5], J Annand[6], J Arrington[7], H B Benaoum[8], F Benmokhtar[9,10], P Bertin[11], W Bertozzi[1], W Boeglin[12], J P Chen[13], Seonho Choi[14], E Chudakov[13], C Ciofi degli Atti[15], E Cisbani[16], W Cosyn[17], B Craver[18], C W de Jager[13], R J Feuerbach[13], E Folts[13], S Frullani[16], F Garibaldi[16], O Gayou[1], S Gilad[1], R Gilman[9,13], O Glamazdin[19], J Gomez[13], O Hansen[13], D W Higinbotham[13], T Holmstrom[20], H Ibrahim[21,34], R Igarashi[22], E Jans[23], X Jiang[9], L Kaufman[24], A Kelleher[20], A Kolarkar[25], E Kuchina[9], G Kumbartzki[9], J J LeRose[13], R Lindgren[18], N Liyanage[18], D J Margaziotis[5], P Markowitz[12], S Marrone[16], M Mazouz[26], D Meekins[13], R Michaels[13], B Moffit[13,20], H Morita[27], S Nanda[13], C F Perdrisat[20], E Piasetzky[3], M Potokar[28], V Punjabi[30], Y Qiang[1], J Reinhold[12], B Reitz[13], G Ron[3], G Rosner[6], J Ryckebusch[17], A Saha[13], B Sawatzky[13,18,31], J Segal[13], A Shahinyan[32], S Širca[28,29], K Slifer[18,31], P Solvignon[13,31], V Sulkosky[1,20], N Thompson[6], P E Ulmer[21], G M Urciuoli[16], E Voutier[26], K Wang[18], J W Watson[4], L B Weinstein[21], B Wojtsekhowski[13], S Wood[13], H Yao[31], X Zheng[1,7] and L Zhu[33]

[1] Massachusetts Institute of Technology, Cambridge, MA 02139, USA
[2] Hampton University, Hampton, VA 23668, USA
[3] Tel Aviv University, Tel Aviv 69978, Israel
[4] Kent State University, Kent, OH 44242, USA
[5] California State University Los Angeles, Los Angeles, CA 90032, USA
[6] University of Glasgow, Glasgow G12 8QQ, UK
[7] Argonne National Laboratory, Argonne, IL 60439, USA
[8] Department of Applied Physics University of Sharjah, Sharjah, UAE
[9] Rutgers, The State University of New Jersey, Piscataway, NJ 08855, USA
[10] University of Maryland, College Park, MD 20742, USA
[11] Laboratoire de Physique Corpusculaire, F-63177 Aubière, France
[12] Florida International University, Miami, FL 33199, USA
[13] Thomas Jefferson National Accelerator Facility, Newport News, VA 23606, USA
[14] Seoul National University, Seoul 151-747, Korea
[15] INFN, Sezione di Perugia , Via A. Pascoli I-06123, Perugia, Italy

[16] INFN, Sezione Sanitá and Istituto Superiore di Sanitá, Laboratorio di Fisica, I-00161 Rome, Italy
[17] Ghent University, Proeftuinstraat 86, B-9000 Gent, Belgium
[18] University of Virginia, Charlottesville, VA 22904, USA
[19] Kharkov Institute of Physics and Technology, Kharkov 310108, Ukraine
[20] College of William and Mary, Williamsburg, VA 23187, USA
[21] Old Dominion University, Norfolk, VA 23508, USA
[22] University of Saskatchewan, Saskatoon, Saskatchewan, Canada S7N 5E2
[23] Nationaal Instituut voor Kernfysica en Hoge-Energiefysica, Amsterdam, The Netherlands
[24] University of Massachusetts Amherst, Amherst, MA 01003, USA
[25] University of Kentucky, Lexington, KY 40506, USA
[26] Laboratoire de Physique Subatomique et de Cosmologie, F-38026 Grenoble, France
[27] Sapporo Gakuin University, Bunkyo-dai 11, Ebetsu 069, Hokkaido, Japan
[28] Institute 'Jožef Stefan', 1000 Ljubljana, Slovenia
[29] Dept. of Physics, University of Ljubljana, 1000 Ljubljana, Slovenia
[30] Norfolk State University, Norfolk, VA 23504, USA
[31] Temple University, Philadelphia, PA 19122, USA
[32] Yerevan Physics Institute, Yerevan 375036, Armenia
[33] University of Illinois at Urbana-Champaign, Urbana, IL 61801, USA
[34] Cairo University, Giza 12613, Egypt

Received 17 February 2014, revised 18 June 2014
Accepted for publication 29 July 2014
Published 27 August 2014

Abstract

The five-fold differential cross section for the $^{12}C(e,e'p)^{11}B$ reaction was determined over a missing momentum range of 200–400 MeV c^{-1}, in a kinematics regime with $x_B > 1$ and $Q^2 = 2.0$ (GeV c^{-1})^2. A comparison of the results with previous lower missing momentum data and with theoretical models are presented. The extracted distorted momentum distribution is shown to be consistent with previous data and extends the range of available data up to 400 MeV c^{-1}. The theoretical calculations are from two very different approaches, one mean field and the other short range correlated; yet for this system the two approaches show striking agreement with the data and each other up to a missing momentum value of 325 MeV c^{-1}. For larger momenta, the calculations diverge which is likely due to the factorization approximation used in the short range approach.

Keywords: cross section, high missing momentum, carbon

(Some figures may appear in colour only in the online journal)

While the independent particle nuclear shell model has enjoyed much success in predicting properties of nucleons in the nucleus up to the Fermi momentum, of approximately 250 MeV c^{-1}, the model breaks down at larger momenta [1] and fails as well for some observables at very low momenta. For example, the observed spectroscopic strength, a multiplicative factor required to match the predicted cross sections with data for valence orbital knockout, averages around 0.65 instead of 1.0 as predicted by the independent particle shell model. One

explanation is that there are nucleon–nucleon correlations present, which are neglected in independent particle calculations. The effect of such correlations would be to deplete valence states occupied below the Fermi momentum and enhance continuum states occupied above the Fermi momentum. In the lab, this translates into shifting strength from low missing momentum ($\vec{p}_m$, the momentum of the undetected residual system) and low missing energy, E_m (which accounts for the separation energy for removing a proton from the target nucleus and any excitation of the residual system) to higher missing momentum and energy in the A $(e,e'p)$ reaction.

Many experiments and much work has been done to study nucleon–nucleon correlations and, while a complete review is outside the scope of this paper [2] provides a clear outline and discussion of the experimental evidence for suitable kinematics for studying nucleon–nucleon correlations. In particular, with a four-momentum transfer squared, $Q^2 = -q_\mu q^\mu = \left|\vec{q}^2\right| - \omega^2 > 1$ $(\text{GeV c}^{-1})^2$ and Bjorken scaling variable $1 < x_B = Q^2/2m_p\omega < 2$, where ω and $\vec{q}$ are the energy and three-momentum transfer respectively from the electron are preferable for studying high p_m nucleon–nucleon correlations. Such kinematics minimize competing effects such as meson-exchange currents, isobar configurations and final state interactions (FSI) which can mask the correlation.

1. Experiment

In this work we examine the ^{12}C$(e,e'p)^{11}$B two-body breakup channel; parallel studies of short-range correlations related to the multi-nucleon knockout reaction channels ^{12}C$(e,e'pp)$ and ^{12}C$(e,e'pn)$ have been published separately [3, 4]. The experiment was performed in Hall A at the Thomas Jefferson National Accelerator Facility (JLab), using the high resolution spectrometers (HRS) [5]. The data were taken at a fixed electron beam energy of 4.627 GeV incident on a 0.25 mm thick natural-carbon foil target. The scattered electrons were detected in the left HRS at a central scattering angle and momentum of 19.5° and 3.762 GeV c^{-1}, respectively. This fixed the electron kinematics, resulting in a central three-momentum transfer of $\left|\vec{q}\right| = 1.66$ GeV c^{-1} and energy transfer of $\omega = 0.865$ GeV, which corresponds to a four momentum transfer squared of $Q^2 \simeq 2$ $(\text{GeV c}^{-1})^2$ and Bjorken scaling variable, $x_B \simeq 1.23$. The knocked-out protons were detected in the right HRS at an angle of $\theta_p = 40.1°$ and a central proton momentum of $\left|\vec{p}_p\right| = 1.45$ GeV c^{-1}. This spectrometer setting provided a continuous coverage of missing momentum $\vec{p}_m = \vec{q} - \vec{p}_p$ from 200–400 MeV c^{-1} for the ^{12}C $(e,e'p)^{11}$B reaction.

The peak in the missing energy distribution shown in figure 1 (left-hand plot) results predominantly from knockout of protons from the $p_{3/2}$ shell, leaving the residual ^{11}B nucleus in its ground state. There is also a *shoulder* of events which is observed around 22 MeV in figure 1; this is due to the ^{11}B nucleus being left in one of several low-lying excited states. Since the missing energy resolution of the experiment (∼3 MeV) was insufficient to separate the individual states of ^{11}B, two simulations were prepared in order to determine correct location of the cut in missing energy which was applied to separate the ground state and excited state contributions. One simulation was fit to the ground state peak and the second simulation was made for the low-lying excited states. By summing the resultant yield from the two simulations and fitting it to the data, the contribution of only the ground state into the *shoulder* region could be separated out. This allowed the application of the missing energy cut at 20 MeV to optimize only the ground state simulation with minimal contamination from the low-lying excited states. In figure 1 (left-hand plot) the red curve shows the results of a

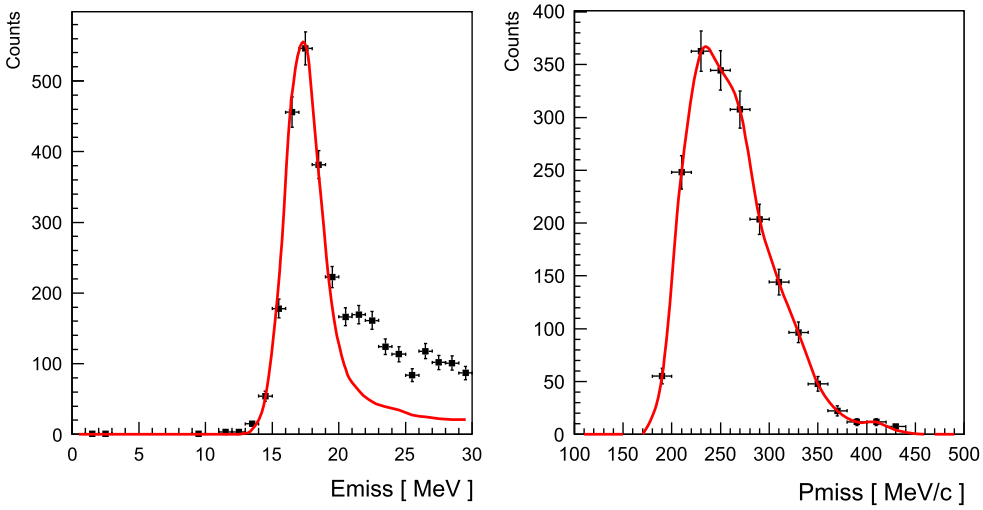

Figure 1. Left: number of counts versus missing energy for the proton spectrometer central momentum of 1.45 GeV c^{-1}. The peak corresponds to proton knockout from the lowest states of carbon, predominantly the $p_{3/2}$state. The red curve shows the simulated data set used for this analysis of the $p_{3/2}$-shell knockout and illustrates the good agreement between the data and the simulation. The simulation curve also shows the tail of events extending out to large missing energy values, which result from real photons radiated out by the electron. Right: the resulting missing momentum distribution after applying a cut on missing energy of 20 MeV to select scattering events to the ^{11}B ground state. The missing momentum data were fit by varying the cross section model in the simulation. The red curve shows the final agreement between the data and the simulation.

simulation normalized to the data that includes radiation of real photons by the electron (the 'radiative tail'). There is a large number of events at missing energies greater than 20 MeV resulting from knockout of protons from the s-shell in addition to knockout of protons from correlated nucleon–nucleon pairs.

2. Data analysis

The $(e,e'p)$ events were selected by placing a 1.1 ns cut around the coincidence timing peak as well as using the HRS pion rejector to suppress the small amount of pion background. The resulting event sample, contained less then 1% random events. The only other cuts on the data were the nominal HRS phase space cuts [5], on momentum, $|\mathrm{d}p/p| < 0.04$ and angular cuts of $|\theta| < 0.05$ radians and $|\phi| < 0.03$ radians about the spectrometers central ray. These cuts discarded events from the edges of the spectrometer acceptances.

A full simulation, including energy losses, multiple scattering, internal and external radiation and spectrometer resolutions was performed. The same set of acceptance cuts, which was applied to the data, was also applied to the simulation. The simulation program **M**onte **C**arlo for $\boldsymbol{e}$, $\boldsymbol{e'p}$ (MCEEP) [6] was used to extract the five-fold differential cross section from the data by using an iterative procedure to adjust the radiated ^{12}C $(e,e'p)$ cross section in the simulation until the simulated yield agreed with the experimental yield in each missing

momentum bin. The right-hand plot of figure 1 shows the final agreement between the simulation (red curve) and the missing momentum data after selecting the ground state data.

The cross section model used in this analysis was based on the factorized distorted wave impulse approximation and is defined as [7]

$$\frac{\mathrm{d}^6\sigma}{\mathrm{d}\Omega_e \mathrm{d}\Omega_p \mathrm{d}E_e \mathrm{d}E_p} = E_p p_p \sigma_{\mathrm{cc2}} S_{\mathrm{D}}\left(\vec{p}_m, E_m\right), \tag{1}$$

where σ_{cc2} is the single-nucleon off-shell cross section prescription of De Forest [7]. The σ_{cc2} prescription is a current-conserving off-shell extrapolation of the on-shell current obtained from the Dirac equation. This prescription includes explicitly the four-momentum transfer (q^μ) in the nucleon current calculation, whereas the σ_{cc1} prescription does not; further details are given in [7]. $S_{\mathrm{D}}(\vec{p}_m, E_m)$ is the proton part of the distorted spectral function and is the probability of detecting a proton in the nucleus with momentum $\vec{p}_m$ and energy E_m.

Integrating equation (1) over the missing energy peak in the discrete part of the ^{11}B spectrum leads to the five-fold differential cross section for a specific state

$$\frac{\mathrm{d}^5\sigma}{\mathrm{d}\Omega_e \mathrm{d}\Omega_p \mathrm{d}E_e} = K\sigma_{\mathrm{cc2}} \int_{\Delta E_m} S_{\mathrm{D}}\left(\vec{p}_m, E_{m'}\right) \mathrm{d}E_{m'}, \tag{2}$$

where $K = E_p p_p \eta^{-1}$ and η is the recoil factor for scattering to a bound state. When integrating equation (1) over the missing energy peak to obtain the five-fold differential cross section, η is the Jacobian which arises and given by

$$\eta = 1 - \frac{E_p}{E_r} \frac{\vec{p}_p \cdot \vec{p}_r}{\left|\vec{p}_p\right|^2}, \tag{3}$$

where E_r and $\vec{p}_r$ are the energy and momentum of the recoiling system. The integral is performed over ΔE_m which is the range of missing energy for the specific state being analyzed to account for the natural width of the final state along with the experimental energy resolution. In this analysis, a range of integration of 0–20 MeV was used to select events from the $p_{3/2}$-shell.

At sufficiently low values of the missing energy, the spectral function is centered around specific values of E_m and it can be assumed to factorize into two functions

$$S_{\mathrm{D}}\left(\vec{p}_m, E_m\right) = \sum_\alpha n_\alpha\left(\vec{p}_m\right) f_\alpha\left(E_m^\alpha\right), \tag{4}$$

where $f_\alpha\left(E_m^\alpha\right)$ is the missing energy distribution for state α and is sharply peaked about E_m^α and $n_\alpha\left(\vec{p}_m\right)$ is the missing momentum distribution for state α. The above considerations allow the cross section to be written as

$$\frac{\mathrm{d}^5\sigma}{\mathrm{d}\Omega_e \mathrm{d}\Omega_p \mathrm{d}E_e} = K\sigma_{\mathrm{cc2}} n_\alpha\left(\vec{p}_m\right) \int f_\alpha\left(E_m\right) \mathrm{d}E_m. \tag{5}$$

Since the missing mass distribution function for a bound state is a delta function, the model cross section can be modified by adjusting the input momentum distribution $n_\alpha(\vec{p}_m)$ in the simulation to agree with the measured cross sections.

An iterative procedure was used to fit the simulated yield to the experimental data. Starting with an initial input momentum function, the simulation was run and the resulting simulated yield as a function of missing momentum compared to the counts in the experimental data, with the same set of cuts being applied to both the simulation and the data. The

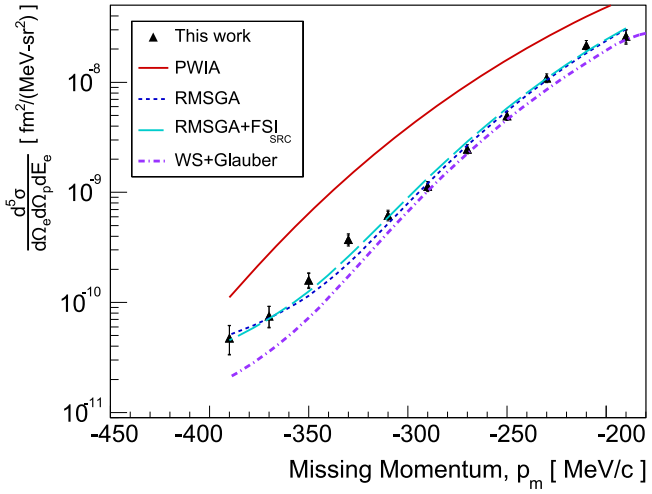

Figure 2. Experimental five-fold differential cross section extracted from the data are compared to several different theoretical calculations. The ground-state wave function for the WS+Glauber calculation includes the effects of correlations, while the one used in the RMSGA calculations does not; no other normalization (spectroscopic factor) has been applied to the calculations. Each data point is plotted at the center of a 20 MeV wide missing momentum bin. The difference between the PWIA calculation and the others demonstrates the importance of properly including final-state interactions to describe the experimental results.

difference between the simulated yield and the experimental data was used to then modify the input momentum function for the next simulation run. This iteration procedure continued until the simulated yield agreed with the experimental data to one percent.

The dominant systematic error in this analysis arose from the selection of scattering events from the ^{12}C $p_{3/2}$-shell to the ^{11}B ground state. This dependence was evaluated by shifting the limit on the E_m by ±1 MeV around 20 MeV and refitting the missing momentum distribution. This yielded a cut dependence of 5.9% in the extracted cross section. Varying other cuts showed no significant change in the resulting cross sections. The next leading source of systematic error was the normalization of the luminosity by comparison with the cross section from hydrogen elastic scattering. For this, the scattering data from a 4 cm extended liquid hydrogen target were compared to MCEEP simulations which used a form factor model derived from a fit to world data [8], this resulted in a 4.5% uncertainty[35]. Other minor sources of uncertainty included an absolute tracking efficiency uncertainty of 1.1%, an uncertainty on the radiative corrections of 1.0% and the uncertainty from the acceptance cuts of <1.0%. The combined total systematic uncertainty was 7.6%.

3. Results

The resulting five-fold differential cross sections as a function of missing momentum is shown in figure 2. The cross section data spans a range of missing momentum of −200 to

[35] This uncertainty is conservative because the hydrogen data were taken using an extended target cell, whereas the physics data were taken on a carbon foil (point) target. Also, a proper background subtraction for the target cell could not be done as the experiment did not take any data with a dummy target cell.

−400 MeV c^{-1}. Although the electron spectrometer had a fixed momentum and angle setting throughout the experiment, the fact that both spectrometers have finite acceptances leads to each data point having slightly different values of Q^2 and ω for each missing momentum bin.

Also shown in figure 2 are four curves produced by calculations utilizing different models. Each calculation has been performed using the appropriate kinematics for each missing momentum bin, rather than only the central spectrometer setting.

The RMSGA and RMSGA + FSI_{SRC} curves in figure 2 are unfactorized relativistic formulations calculations by W Cosyn and J Ryckebusch [9]. The bound-state wave functions are solutions to the Dirac equation with scalar and vector potentials fitted to ground-state nuclear properties. The final-state interactions are modelled on rescattering of a fast proton from a composite target containing $A - 1$ *frozen* spectator nucleons. The curve labelled 'RMSGA+FSI_{SRC}' differs from the 'RMSGA' calculation in that it has been extended to include short-range correlation effects in the final-state interactions [10]. These correlations create local fluctuations in the nuclear density, modifying the attenuation of the scattered proton in the nuclear medium.

The WS+Glauber curve in figure 2 corresponds to a factorized calculation by M Alvioli, C Ciofi degli Atti and H Morita [11]. This model uses many-body variational correlated wavefunctions resulting from a cluster expansion solution of the non-relativistic Schroedinger equation with realistic nucleon–nucleon interactions and Woods–Saxon (WS) single particle wavefunctions [11]. The final-state interactions are modeled using an improved Glauber approach [12] to describe the rescattering of the knocked-out proton [13–15]. This calculation includes ground state correlations in the initial wave function which result in a reduction of the cross section by a factor of 0.8. This has the effect of reducing the occupation number of the $1p_{3/2}$ shell predicted by an independent particle shell model.

Plane wave impulse approximation (PWIA) calculations were done independently by both groups to ensure the same baseline calculation and gave the same result which is why only one PWIA curve is shown in figure 2. More striking is the agreement between the WS+Glauber calculation and full the RMSGA calculation. Only at the highest momenta does one start to see a deviation between the curves and preference of the data to the RMSGA calculation. This is likely due to the fact that at this time the WS+Glauber calculation is factorized while the RMSGA is unfactorized.

The experimental distorted momentum distribution is extracted from the cross section data by dividing out the kinematic factor and the single nucleon off-shell cross section terms, σ_{cc2}, in equation (2). This was accomplished by running another MCEEP simulation, with all of the input parameters unchanged, except now with a uniform input momentum function. This meant that all of the same averaging over the same missing momentum bins as was done for the cross section extraction was repeated for this simulation to generate just the kinematic factor and the single nucleon off-shell cross section. The distorted momentum distribution is then given by

$$n_{\text{distorted}}(p_m) = \left\langle \frac{\mathrm{d}^5\sigma}{\mathrm{d}\Omega_e \mathrm{d}\Omega_p \mathrm{d}E_e} \right\rangle_{\text{exp}} \Big/ \left\langle K\sigma_{cc2} \right\rangle_{\text{unit}}. \tag{6}$$

The experimental distorted momentum distribution from this experiment covers a range in missing momentum of −200 to −400 MeV c^{-1}, which overlaps with data from a previous experiment in Hall C at JLab [16]. A comparison of the experimental distorted momentum distributions from both experiments along with calculated momentum distributions arising from the models used to calculate the cross sections in figure 2 are shown in figure 3. The data from the Hall C experiment shown here were taken at $Q^2 = 1.8$ (GeV c^{-1})^2 and include a cut

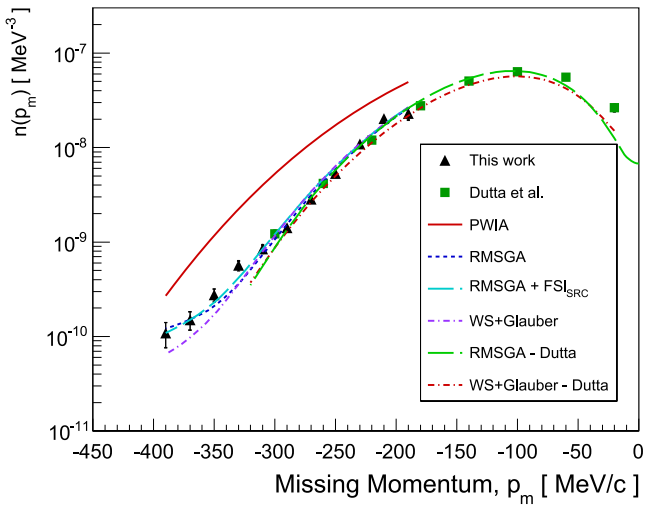

Figure 3. Comparison of experimental distorted momentum distribution extracted from two different experiments with theoretical calculations based on the RMSGA and WS +Glauber approaches, as well as a simple PWIA calculation. The agreement with the experimental data shows the same general trends as observed in the cross section comparison and shows in general this reaction can be well described with either a mean field or WS+Glauber calculation over nearly the entire momentum range. Note, the curves labelled *'Dutta'* were made using the kinematics from the Hall C experiment [16], which are slightly different from our kinematics. The error bars for both sets of data are plotted, although the logarithmic scale makes their observation difficult for all but the largest errors.

on missing energy of $15 < E_m < 25$ MeV to select the p-shell; however, this missing energy range does include some contribution from s-shell knockout. The Hall C analysis includes a factor of $(2j + 1)$ for the multiplicity of the shell being considered. This analysis extracted the cross section per nucleon and so to make this comparison, our data are multiplied by a factor of 4.

The RMSGA and WS+Glauber calculations were performed for the applicable kinematics from both experiments for the data shown and hence there are two different sets of curves in figure 3. As figure 3 shows, the two experiments agree in the overlap momentum region from −200 to −300 MeV c^{-1}. The data from this experiment extends the experimental momentum distribution to −400 MeV c^{-1}. The resulting momentum distributions from the PWIA, RMSGA and WS+Glauber calculations are compared to the data in figure 3. The RMSGA and WS+Glauber calculations are in good agreement with the data from both experiments and each other up to a missing momentum around 325 MeV c^{-1}, where they start to diverge slightly likely due to the factorization approximation in the WS+Glauber calculation.

Since our data is predominantly from the $p_{3/2}$ shell, the occupation number for that shell in the carbon ground state can be inferred from the theoretical calculation. The number of protons in a sub-shell of the ground state is given by the integral of the momentum distribution of that shell. For our data, since we only have experimental data covering the missing momentum range of −200 to −400MeV c^{-1}, and not the full momentum range, the integral has to be performed using the fact that we have good agreement with the theoretical models. For this result, the occupation number was determined by integral of the

Table 1. Results for the $^{12}C(e, e'p)^{11}B$ reaction data from the highest proton momentum spectrometer setting. The statistical error quoted for the cross section is the same for the extraced momentum distribution. The cross section numbers are given by the experimentally-normalized Monte Carlo simulation at the central value of the kinematics quoted for each missing momentum bin. The central values of Q^2 and ω and their corresponding RMS widths σ_Q^2 and σ_ω are given for each missing momentum bin. Not shown is the global systematic error of 7.6%.

p_m	$\frac{d^5\sigma}{d\Omega_e d\Omega_p dE_e} \pm \delta_{stat}$	$n(p_m)$	$\bar{Q}^2 \pm \sigma_{Q^2}$	$\bar{\omega} \pm \sigma_\omega$
(MeV c^{-1})	(fm^2 (MeV-sr^2)$^{-1}$)	(MeV^{-3})	((GeV c^{-1})^2)	(MeV)
190	2.62e-08 ± 13.5%	2.29e-08	1.70 ± 0.018	852 ± 4.2
210	2.18e-08 ± 6.3%	2.03e-08	1.72 ± 0.033	846 ± 8.4
230	1.09e-08 ± 5.3%	1.09e-08	1.74 ± 0.046	841 ± 12.5
250	4.95e-09 ± 5.4%	5.31e-09	1.77 ± 0.060	836 ± 16.6
270	2.47e-09 ± 5.7%	2.85e-09	1.80 ± 0.075	830 ± 20.7
290	1.13e-09 ± 7.0%	1.42e-09	1.83 ± 0.088	824 ± 23.9
310	6.20e-10 ± 8.3%	8.48e-10	1.87 ± 0.103	819 ± 26.0
330	3.73e-10 ± 10.2%	5.66e-10	1.92 ± 0.117	815 ± 27.1
350	1.60e-10 ± 14.5%	2.76e-10	1.98 ± 0.128	814 ± 27.8
370	7.56e-11 ± 21.2%	1.50e-10	2.05 ± 0.134	813 ± 28.0
390	4.77e-11 ± 29.3%	1.09e-10	2.11 ± 0.130	813 ± 27.7

WS+Glauber calculation over a range of missing momentum from −20 to −400 MeV c^{-1}. This integral is precisely 3.2, but is the total occupation number for the p-shell. This occupation number arises from 4 × 0.8, corresponding to the factor of 0.8 which was already included in the initial state wavefunction to account for short-range correlations. This does not tell us anything about separate occupation probabilites of either the $p_{3/2}$ or $p_{1/2}$ shells in carbon as these are also governed by long-range correlations. However, shell model calculations by other groups have shown that ∼70% of p-shell protons occupy the $p_{3/2}$ ground state. This means the integral value is further reduced by a factor of 0.7, resulting in an occupation number of 2.24 for the $p_{3/2}$ shell.

For completeness, the experimental cross section and extracted momentum distribution results are shown in table 1. The statistical uncertainties for each data point are quoted, with the same statistical uncertainty applicable to both the cross section and the momentum distribution. The systematic uncertainty, includes normalization, kinematic and event selection uncertainties which were all added together in quadrature, to produce a global value of 7.6%. The quoted cross section numbers are given by the experimentally-normalized Monte Carlo simulation at the quoted central kinematic values for each bin. The average values of Q^2 and ω as well as their RMS widths for each missing momentum bin are also provided.

4. Conclusions

In summary, the experimental five-fold differential cross section for the $^{12}C(e,e'p)^{11}B$ reaction has been extracted in a previously unexplored kinematic region. The data extends over a range of missing momenta from −200 to −400 MeV c^{-1}. A comparison of our data with calculations which include final-state interactions by two different approaches demonstrates the failure of PWIA while highlighting the ability of modern mean field and short range correlated calculations to both discribe the $^{12}C(e, e'p)^{11}B$ reaction over a large range of the

missing momentum. The variations of the WS+Glauber calculations from the data at missing momenta above 325 MeV c^{-1} likely is the result of the factorization approximation in these calculations.

The experimental distorted momentum distribution was also extracted from the cross section data and compared with a previous experiment in Hall C at JLab. The data from both experiments are consistent for the region of missing momentum where they overlap. The theoretical calculations also show good agreement with the data up to a missing momentum around 325 MeV c^{-1}, where they diverge slightly. In general the agreement of the data with both the short range correlated and mean field approaches is very good. Using the agreement of our data with the calculations, the occupation number of the $p_{3/2}$ shell was inferred and found to be 2.24.

Acknowledgments

We would like to acknowledge the contribution of the Hall A collaboration, the Hall A technical staff and the accelerator operations staff. This work was supported by the Israel Science Foundation, the US-Israeli Bi-national Scientific Foundation, the UK Engineering and Physical Sciences Research Council, the US National Science Foundation, the US Department of Energy grants DE-FG02-94ER40844, DE-AC02-06CH11357, DE-FG02-94ER40818, and US DOE Contract No. DE-AC05-84150, Modification No. M175, under which the Southeastern Universities Research Association, Inc. operates the Thomas Jefferson National Accelerator Facility.

References

[1] Kelly J J 1996 Nucleon knockout by intermediate-energy electrons *Adv. Nucl. Phys.* **23** 75–294
[2] Arrington J, Higinbotham D W, Rosner G and Sargsian M 2012 Hard probes of short-range nucleon–nucleon correlations *Prog. Part. Nucl. Phys.* **67** 898–938
[3] Shneor R *et al* 2007 Investigation of proton-proton short-range correlations via the 12C(e, $e'pp$) reaction *Phys. Rev. Lett.* **99** 072501
[4] Subedi R *et al* 2008 Probing cold dense nuclear matter *Science* **320** 1476–8
[5] Alcorn J *et al* 2004 Basic instrumentation for Hall A at Jefferson lab *Nucl. Instrum. Methods* A **522** 294–346
[6] Ulmer P E *et al* MCEEP: Monte Carlo for (e, $e'p$) experiments (http://hallaweb.jlab.org/software/mceep/mceep.html)
[7] De Forest T 1983 Off-shell electron nucleon cross-sections. The impulse approximation *Nucl. Phys.* A **392** 232–48
[8] Arrington J 2004 Implications of the discrepancy between proton form-factor measurements *Phys. Rev.* C **69** 022201
[9] Ryckebusch J *et al* 2003 Relativistic formulation of Glauber theory for A(e, $e'p$) reactions *Nucl. Phys.* A **728** 226–50
[10] Cosyn W, Martínez M C and Ryckebusch J 2008 Color transparency and short-range correlations in exclusive pion photo- and electroproduction from nuclei *Phys. Rev.* C **77** 034602
[11] Alvioli M, Ciofi degli Atti C and Morita H 2005 Ground-state energies, densities and momentum distributions in closed-shell nuclei calculated within a cluster expansion approach and realistic interactions *Phys. Rev.* C **72** 054310
[12] Glauber R J 1959 *Lectures in Theoretical Physics* (New York: Interscience)
[13] Morita H, Ciofi degli Atti C and Treleani D 1999 A Realistic study of the nuclear transparency and the distorted momentum distributions in the semiinclusive process He-4(e, $e'p$)X *Phys. Rev.* C **60** 034603
[14] Ciofi degli Atti C, Kaptari L P and Morita H 2007 Hadron propagation in medium: the exclusive process A(e, $e'p$)B in few-nucleon systems *Nucl. Phys.* A **782** 191–8

[15] Ciofi delgi Atti C and Kaptari L P 2008 A Non factorized calculation of the process He-3(e, e' p) H-2 at medium energies *Phys. Rev. Lett.* **100** 122301
[16] Dutta D *et al* 2003 Quasielastic (e, $e'p$) reaction on $C12$, $Fe56$, and $Au197$ *Phys. Rev.* C **68** 064603